Double-Exposure Grayscale Photolithography

Lance Mosher, Christopher M. Waits, *Student Member, IEEE*, Brian Morgan, *Member, IEEE*, and
Reza Ghodssi, *Member, IEEE*

Abstract—A double-exposure grayscale photolithography technique is developed and demonstrated to produce three-dimensional (3-D) structures with a high vertical resolution. Pixelated grayscale masks often suffer from limited vertical resolution due to restrictions on the mask fabrication. The double-exposure technique uses two pixelated grayscale mask exposures before development and dramatically increases the vertical resolution without altering the mask fabrication process. An empirical calibration technique was employed for mask design and was also applied to study the effects of exposure time and mask misalignment on the photoresist profile. This technology has been demonstrated to improve the average step between photoresist levels from 0.19 to 0.02 μm and the maximum step from 0.43 to 0.2 μm compared to a single pixelated exposure using the same mask design.   **[2008-0164]**

Index Terms—Grayscale lithography, microelectromechanical systems (MEMS), micromachining, three-dimensional (3-D) lithography.

I. INTRODUCTION

THE DESIGN of traditional microelectromechanical systems (MEMS) has been partially restricted by the fabrication limitations of technology that was initially developed for the IC industry. Common photolithography is a widely accepted and powerful patterning technology but only produces planar structures. This restriction is not prohibitive for IC fabrication, but it is a significant limitation for MEMS technologies that may greatly benefit from three-dimensional (3-D) geometries. As new 3-D photolithography techniques emerge, a variety of applications have taken advantage of this new design capability. Turbomachinery applications [1] can utilize sloped sidewalls to increase compressor performance. Encapsulated microfluidic channels can be fabricated with a single photolithography step [2]. Other applications include the fabrication of photonic crystals [3] and phase Fresnel lenses [4], which cannot be realized without 3-D forming capabilities.

In contrast to binary photolithography, 3-D photolithography methods use variable-exposure techniques to produce vertically shaped photoresist profiles. Commonly, 3-D photolithography is achieved using a variable-dose exposure, called grayscale photolithography, to control the development depth in photoresist [5]. Regions exposed to a given dose will develop to a corresponding photoresist thickness, termed a gray level. A higher dose penetrates the photoresist deeper and therefore creates a lower gray level when using positive-tone photoresist. The remaining 3-D pattern can then be either transferred into a substrate via directional dry etching [1] or used as the structural material itself.

Current 3-D photolithography technologies can be divided into three primary groups: multiple-step, direct-write, and grayscale mask photolithography. Multiple-step photolithography utilizes several exposures using conventional optical masks [2], [3], [6], but each exposure produces a different gray level in the photoresist. With this technique, n masks have been demonstrated to produce $n + 1$ gray levels, but alignment and edge effects limit the total number of exposures. The maskless direct-write process uses a writing beam to directly transfer a variable-dose pattern into the photoresist [7]–[13]. Grayscale mask photolithography uses a conventional photolithography tool with a specialized grayscale optical mask [14]–[22]. Grayscale masks contain variable-transmission patterns that transmit part of the ultraviolet (UV) light intensity to create variable-relief structures. Each photolithography technique has advantages and disadvantages that make it suited for different applications. The goal of this paper is to develop a high-throughput technology capable of realizing 3-D structures with a high vertical resolution. Photolithography using grayscale masks provides a much higher throughput than direct-write methods but is also capable of realizing structures with a much higher vertical precision than multiple-step photolithography. Therefore, grayscale mask photolithography is ideal for this paper.

The mechanisms to control the UV intensity in grayscale mask photolithography have been demonstrated using both pixelated [14]–[20] and continuous-tone [21], [22] grayscale optical masks. Pixelated grayscale masks control the UV dose by diffraction through pixels that are below the resolution of the photolithography tool. Continuous-tone masks are fabricated by directly writing the optical density onto a mask coated with a proprietary energy-beam-sensitive material that controls the UV absorption. Both continuous-tone and pixelated masks can be used to fabricate structures on the order of tens of micrometers, but continuous-tone masks use a proprietary writing technology that is limited to 5- or 6-in mask plates. Pixelated grayscale masks may be written with conventional mask writers and are compatible with any plate dimension. While this is

L. Mosher is with the Lockheed Martin Space Systems Company, Newtown, PA 19104 USA (e-mail: lance.mosher@lmco.com).

C. M. Waits and B. Morgan are with the U.S. Army Research Laboratory, Adelphi, MD 20783 USA.

R. Ghodssi is with the MEMS Sensors and Actuators Laboratory, Department of Electrical and Computer Engineering, Institute for Systems Research, University of Maryland, College Park, MD 20742 USA.
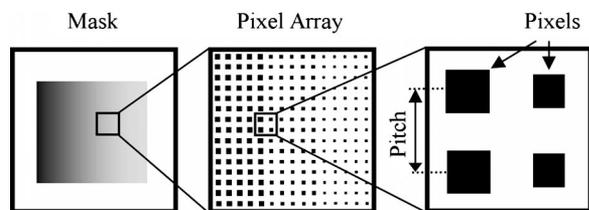
Fig. 1.   Top–down schematic of a pixelated grayscale mask. Closer examination reveals the structure of the individual pixels.
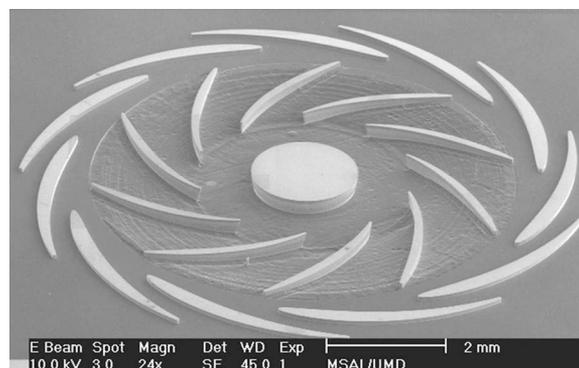

Fig. 2.   SEM of the 3-D microcompressor prototype fabricated using pixelated grayscale photolithography and deep reactive-ion etching.
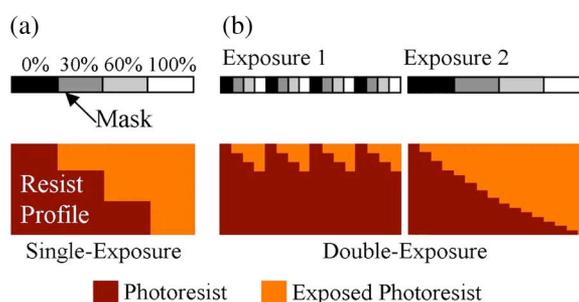

Fig. 3.   Profile view of (a) single-exposure photolithography using a mask with four pixel sizes, producing four gray levels. (b) Double exposure produces 16 gray levels using two exposures with the same number of pixel sizes.

beneficial, pixelated grayscale photolithography has a much lower vertical resolution than continuous-tone masks and is therefore not well suited for many applications.

As a solution to this limitation, the focus of this paper is to present the development of a new photolithography technique, termed double-exposure grayscale photolithography. This technique combines multiple-step photolithography with pixelated grayscale masks. Multiple exposure steps have been demonstrated to improve the vertical resolution of conventional masks, and similarly, double-exposure photolithography extends the resolution of pixelated grayscale masks. This paper presents an overview of pixelated grayscale photolithography, followed by a detailed description of the double-exposure photolithography technique. An empirical calibration technique required to design double-exposure masks is also reported. The first double-exposure grayscale structures have been fabricated as a technology demonstration and have been analyzed to verify the calibration. Finally, the effects of mask alignment and solutions to tolerate misalignment are discussed.

II. PIXELATED GRAYSCALE PHOTOLITHOGRAPHY

Pixelated grayscale masks are fabricated using high-resolution mask writers capable of submicrometer feature sizes. Unlike common mask features, the pixels are intentionally designed to be below the resolution limit of the photolithography system. The pixels on the mask (Fig. 1) vary the transmitted UV light intensity when the mask is exposed in a projection photolithography system. The subresolution pixels diffract the UV light, and the projection optics filter out the spatial information and transmit only a diminished UV intensity [5]. The amplitude of the intensity is controlled by the pixel size and the pitch. Projection photolithography is required to achieve sufficient diffraction through the pixel grid, which makes this technique incompatible with contact photolithography. Only a finite number of pixel sizes are possible due to mask writing limitations. In addition, each pixel size corresponds to a unique gray level, allowing only a finite number of possible gray levels. As a result, desired 3-D structures must be approximated by the available set of gray levels.

The degree of approximation required for pixelated grayscale photolithography is prohibitive for applications that require high vertical resolution. For example, 3-D profiles can be desirable for turbomachinery applications [23]. The microcompressor prototype in Fig. 2, related to the work in [1], was fabricated using pixelated grayscale photolithography and transferred into silicon using a two-step etch process. The inwardly sloping profile maintains a constant cross-sectional area

between blades on the rotating compressor, which increases the compressor efficiency. However, the current vertical resolution of this pixelated grayscale technology is not sufficient to meet the specifications of this device. Approximating the desired slope produces a stepped profile that restricts fluid flow and decreases device performance.

The limitation in the vertical resolution is imposed by the mask fabrication process and the projection photolithography tool. The resolution of the projection system determines the upper limit on the pixel size. Typical low-resolution systems, such as the $5\times$ projection tool used in this paper, have resolutions near 0.6 μm on the wafer. This allows pixel sizes up to 3 μm before spatial information from individual pixels begins to transfer. The mask fabrication limits the minimum pixel size and the minimum difference between pixel sizes. The projection photolithography tool and mask process enables grayscale designs using 15 square pixel sizes ranging from 0.6 to 2.0 μm.

III. DOUBLE-EXPOSURE GRAYSCALE PHOTOLITHOGRAPHY

Double-exposure grayscale photolithography was developed to improve the vertical resolution compared to a single exposure without increasing the mask fabrication complexity. Similar to multiple-step techniques, the process consists of two aligned exposures before development, but each exposure uses a grayscale mask in place of a binary mask (Fig. 3). Unlike previous demonstrations of multiple-step lithography, both

exposures are overlaid above the same location on the photoresist. Examples of multiple-step photolithography in the literature use adjacent exposures, where each step is applied to unexposed photoresist. Double-exposure photolithography attempts a new phenomenon. Instead of exposing the photoresist down to the substrate or partially to create a gray level, two partial exposures are superimposed to create a gray level that is not achievable using a single exposure [24]. Therefore, the final structure is composed of a combination of both partial exposures, as shown in Fig. 3(b). Any pixel size used in the first exposure may be followed by any other pixel size in the second exposure. If two different exposure times are used with n pixel sizes, double exposure will produce n^2 gray levels. However, if the exposure times are equal, the number of gray levels will be reduced.

The application of double-exposure grayscale photolithography requires the design of two pixelated masks. Mask design necessitates an understanding of how each pixel will affect the final photoresist height. Process calibration is increasingly complicated because each point on the photoresist is exposed with two different pixel sizes and two different exposure times. The first step is to examine the exposure mechanics and define a single variable, the double-exposure dose, which depends on the pixel size and exposure conditions and can be experimentally compared to the photoresist height. The next step is to expose a calibration structure and collect empirical data. These data are then related to the double-exposure dose to develop a numerical relationship between the photoresist height and the exposure conditions, called the calibration curve. After a reliable calibration is obtained, a set of pixelated masks can be designed to fabricate nearly any arbitrary geometry.

A. Theory

In order to design a pixelated mask, it is important to quantify the relationship between the pixel size and the resulting photoresist height. This requires an understanding of the photoresist exposure process, which differs for positive- and negative-tone photoresists. Only positive-tone photoresist was used in this work, but grayscale lithography has been previously demonstrated using negative-tone photoresist [2], [3], and therefore, it is reasonable to assume that double exposure would have a similar effect on negative-tone photoresist. The exposure kinetics of positive photoresist is governed by Beer's law

$$I(z) = I_s \exp(-\alpha \cdot z) \tag{1}$$

where $I(z)$ is the intensity at depth z, I_s is the intensity at the photoresist surface, and α is the absorption coefficient of the photoresist. The absorption coefficient can be determined from the Dill parameters [25] of the photoresist, as described by Kim *et al.* [26]. The photoresist is fully exposed when the dose is greater than the dose-to-clear E_0. The dose d is defined with the exposure time t as

$$d(z) = I(z) \cdot t. \tag{2}$$

The dose-to-clear is a well-known property that specifies the minimum energy required to remove photoresist during de-velopment. The maximum development depth $z_{\max}$ can be obtained from (1) and (2) by substituting the dose with the dose-to-clear $(d(z) = E_0)$

$$z_{\max} = \frac{1}{\alpha} \ln\left(\frac{t \cdot I_s}{E_0}\right). \tag{3}$$

Unfortunately, this theoretical approach is not sufficient to calculate the exposure depth using the tools available for this work. For example, slight variations in the photoresist deposition, development temperature, and humidity can affect the final photoresist profile. Therefore, a calibration technique was selected to relate the pixel size on the mask to the corresponding gray-level height, as demonstrated by Morgan *et al.* [4].

In this empirical calibration scheme, the dose is calculated and directly compared to the resulting photoresist height. The incident UV intensity I_0 is constant during the exposure, but the surface intensity I_s is controlled by the amount of light transmitted through optical mask. The UV transmission is determined by the size of the pixels on the mask or, specifically, the transparent area surrounding the pixel, given by

$$I_s = I_0 \frac{p^2 - l^2}{p^2} \tag{4}$$

where l is the length of the square pixel and p is the spacing between pixels on the mask, which is termed the pitch. In general, dose is defined as the product of relative intensity and exposure time. Double exposure uses two exposure intensities, with two doses, so the double-exposure dose d_{de} is defined as the sum of the independent dose for each exposure

$$d_{\mathrm{de}} = I_{s1}t_1 + I_{s2}t_2 \tag{5}$$

where the subscript indicates the first or second exposure.

IV. Calibration and Design

Double-exposure grayscale photolithography is the first technique that demonstrates the use of two partial exposures that are overlaid to produce an intermediate development depth. Therefore, this technique requires a more sophisticated calibration approach compared to single-exposure photolithography. For example, it is important to examine how the first exposure modifies the exposure kinetics of the photoresist and if that will affect subsequent exposures. Equation (5) only applies if the order of the exposures does not impact the corresponding gray-level height. Therefore, it is necessary to observe if the exposures commute. The exposure time is also more complicated using double-exposure photolithography. The total exposure time is selected for the photolithography process itself, but the individual exposure times can be changed freely, making it important to analyze the effect of changing the individual exposure times.

A. Exposure Commutability

Multiple-step photolithography has been demonstrated with binary masks, but no previous results have shown the effect of

superimposed grayscale exposures. Therefore, it is necessary to investigate if and how the order of exposure affects the final photoresist height. As shown in (1), the intensity changes as a function of depth in the photoresist and the absorption coefficient. However, due to bleaching effects, the absorption coefficient changes as the photoresist is exposed [26]. Since the double-exposure dose given in (5) is only valid if the two exposures are commutative, the change in the absorption coefficient must have a negligible effect on the intended exposures. We used a simple experimental approach to test the commutability of the exposures within the typical dose range. Pairs of photoresist test pads were exposed with the same two exposure doses, but in opposite order. These exposure opposites were created using all pixel size combinations. If the exposures are commutative, the height of opposite exposures will be identical. The average difference in photoresist height of such opposite exposures was only 1.5% of the total photoresist height. This value is on the order of the average height difference for two identical gray levels. While this result holds for the typical dose range used in these experiments, a different exposure process may cause the absorption coefficient to change significantly, resulting in a noncommuting exposure. Therefore, the commutability of the exposures must be examined prior to developing a calibration curve using this method. Photoresist kinetic modeling software can be used to determine the range of commutability for different photoresist chemical compositions as well as exposure processes.

B. Calibration

Mask design is not possible until the double-exposure grayscale technology is calibrated with a defined relationship between the pixel size and the resulting photoresist height. Experimental data for empirical calibration were collected using a characterization mask with 15 square pixel sizes. A calibration structure was designed on a test mask to provide a means to measure the gray-level heights resulting from all pixel size combinations. The structure contained a grid of test pads, which are 100-μm squares of the same pixel size. The pads were arranged in a 15 × 15 grid, as shown in Fig. 4, to overlap all combinations of pixel sizes using double-exposure photolithography. The combination of both exposures results in 225 double-exposure combinations. After exposure and development, a stylus profilometer was used to measure the height of the fabricated gray levels. An empirical relationship could then be extracted by examining the correlation between the relative double-exposure dose calculated from (5) and the measured gray-level height.

Due to the exponential nature of the exposure kinetics, the data were fit to an exponential equation of the form

$$depth = y_0 + A \cdot [1 - \exp(-dose \cdot B)]. \tag{6}$$

The double-exposure dose was calculated, as given in (5), and normalized to unity. Fig. 5 shows this exponential fit, where $y_0 = -8.85$, $A = 15.11$, and $B = 3.3$. The resulting empirical calibration curve is given by

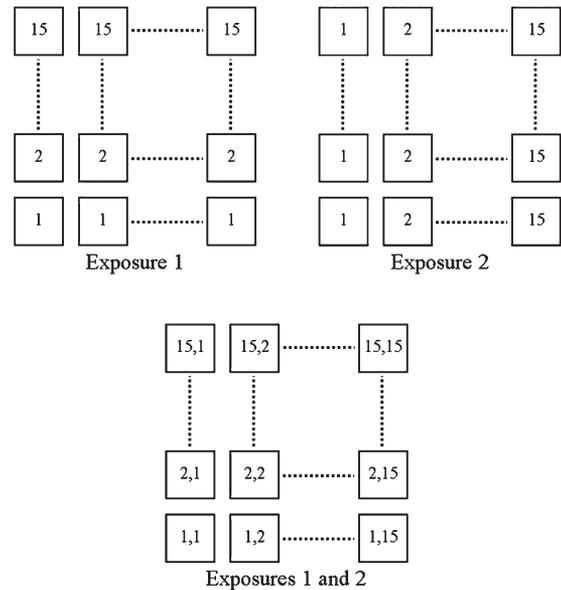$$depth = -8.85 + 15.11 \cdot [1 - \exp(-dose \cdot 3.30)]. \tag{7}$$

Fig. 4. Grayscale test pads are grouped in rows for the first exposure and columns for the second exposure. The pixel size is represented by numbers 1–15. When the two exposures are overlaid, all possible test pad combinations produce 225 gray levels.
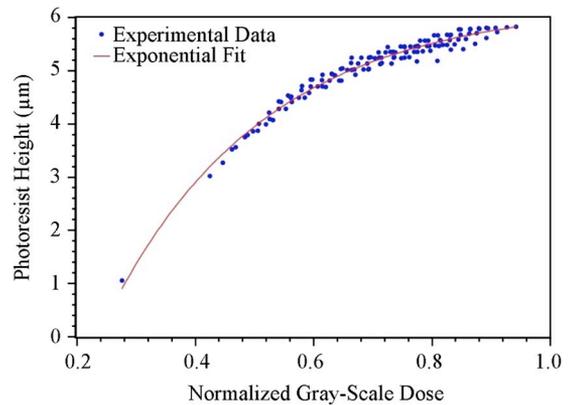

Fig. 5. Double-exposure calibration data are fit to an exponential equation to determine the relationship between the normalized dose and the height of the corresponding gray level.

C. Exposure Time Ratio

While the relationship from Fig. 5 is sufficient to design a double-exposure grayscale mask, the ratio between the exposure times should be optimized. The total exposure time is usually determined from the existing photolithography process, including the photoresist thickness and the desired development time. However, the individual exposures are not constrained, and changing the individual exposures will change the vertical distribution of gray levels in the photoresist. Therefore, the optimum exposure times for both exposures must be determined to use the calibration curve for mask design. Since the total exposure time is fixed and the order of exposures does not matter, both individual exposures can simply be expressed as the ratio between the two exposure times. The effect of changing the exposure time ratio was examined by using (5) to calculate all possible dose values when given an exposure ratio. The resulting dose values were then converted to predicted

photoresist heights using the calibration from (7). The optimum exposure time ratio was selected to achieve the most uniform vertical distribution of gray levels. This was determined by minimizing the average step height between gray levels. The optimum exposure time ratio was calculated to be $1.78 : 1$, which was used for future mask designs.

D. Mask Design

A set of test masks were designed using the calibration curve and the optimum exposure times described earlier to demonstrate the realization of double-exposure structures and to validate the calibration approach. The masks utilized $n = 15$ square grayscale pixel sizes ranging from 0.6 to 2.0 μm with a 0.1-μm difference between pixel sizes. Double-exposure photolithography was predicted to yield $n^2 = 225$ gray levels [27]. Several linear wedge structures of various lengths and heights were designed on the masks. Since millions of pixels must be precisely placed, each structure was designed automatically using a computer script. The script first calculated all possible gray levels by using the calibration curve from (7), the exposure times, and the pixel sizes for the mask. The desired structure was then approximated using the available gray levels, and the mask layout file was produced. Fabrication began by spinning a 6-μm layer of Clariant's AZ9245 positive-tone photoresist. The wafer was then exposed in a GCA i-line wafer stepper for both exposures and developed in a $1 : 4$ AZ400 K solution for 6 min.

V. RESULTS AND DISCUSSION

A. Improved Vertical Resolution

Using the same set of 15 pixel sizes and the same exposure and development procedure, double exposure produced 225 gray levels compared to 15 gray levels using a single exposure. Double-exposure decreased the average step height from 0.19 to 0.02 μm, and the maximum step height decreased from 0.43 to 0.2 μm. This increase in vertical resolution will enable the successful realization of the microcompressor shown in Fig. 2 to within the required specifications.

The improved vertical resolution achieved with double-exposure grayscale photolithography enables realization of structures that were never possible using pixelated grayscale technology. A wedge structure was fabricated using both single- and double-exposure techniques and compared to the ideal wedge shape. SEM images of the photoresist surface verify that the single-exposure structure (Fig. 6) contains fewer gray levels than a wedge fabricated with double-exposure photolithography (Fig. 7). As shown in Fig. 8, the structure fabricated with double-exposure grayscale photolithography more closely matches the ideal wedge shape. The average differences between the fabricated structure and the ideal wedge profile were 0.98 μm (33% of structure height) using single-exposure grayscale photolithography and 0.17 μm (6% of structure height) using double-exposure grayscale photolithography.

B. Mask Misalignment

The double-exposure profile shown in Fig. 8 is closer to the designed structure than the single-exposure profile but exhibits
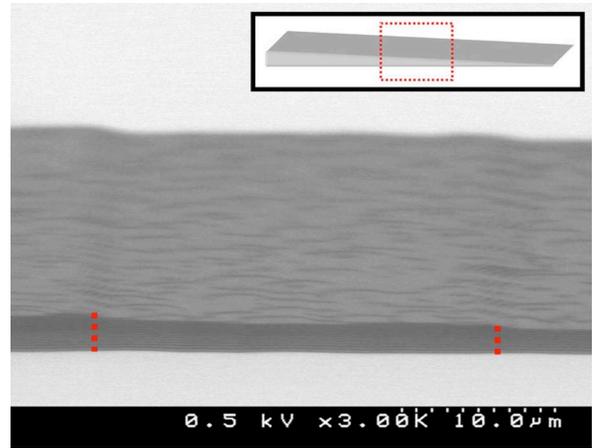

Fig. 6.   SEM of a wedge fabricated with single-exposure photolithography. The boundaries between the three gray levels are outlined by red dotted lines. The inset depicts the portion of the structure shown.
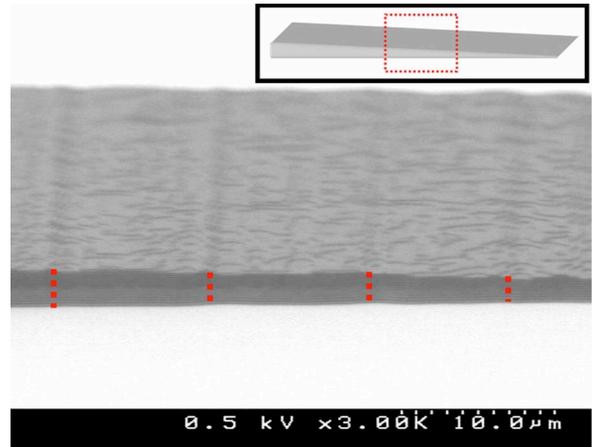

Fig. 7.   SEM of a wedge fabricated with double-exposure photolithography. The boundaries between the five gray levels are outlined by red dotted lines. The inset depicts the portion of the structure shown.
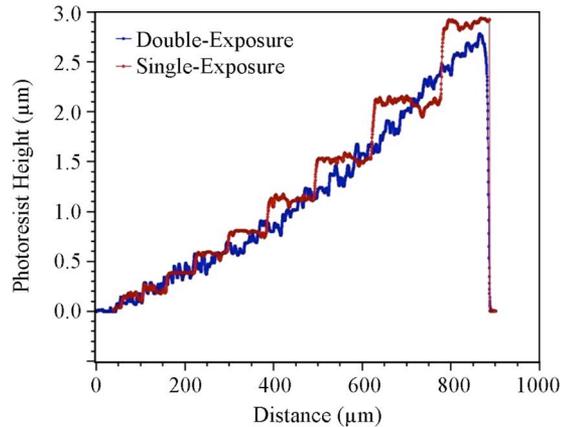

Fig. 8.   Contact profilometer scan of a double- and a single-exposure wedge structure in photoresist, showing an increased resolution in the vertical step height.

increased roughness. To explore the cause of this roughness, we developed a simulation to investigate the effect of misalignment between the two exposures, as shown in Fig. 9. If the second exposure is misaligned from the first, erroneous pixel
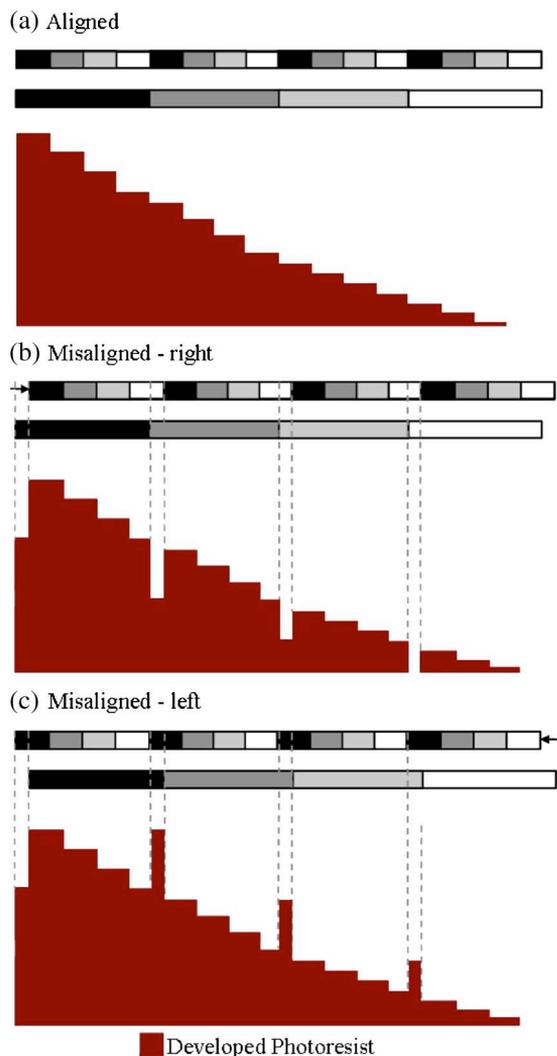
Fig. 9. Illustration showing (a) an aligned double-exposure profile, (b) a misaligned double-exposure profile with valleys caused by misaligned regions, and (c) a misaligned double-exposure profile with peaks caused by misaligned regions.
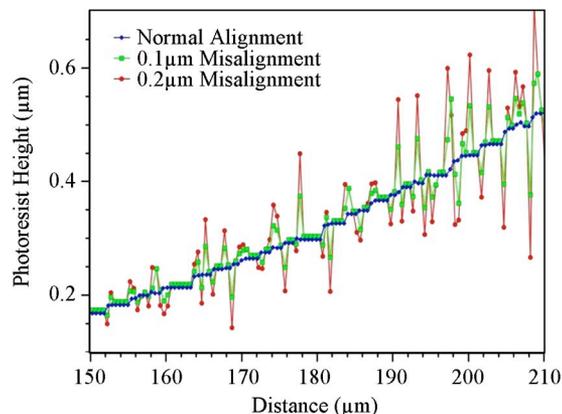

Fig. 10. Simulated profile demonstrating increasing roughness with greater misalignment.
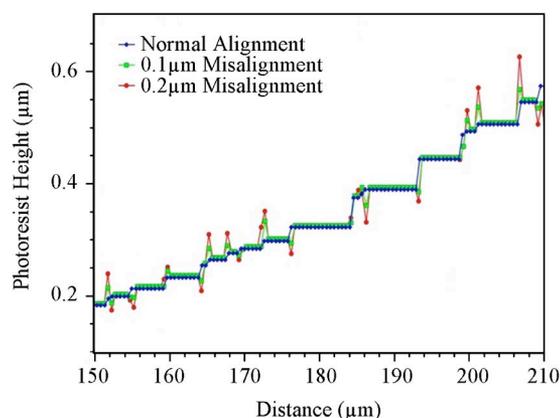

Fig. 11. Simulated profile after applying the design rule to the simulation, demonstrating fewer irregularities at the expense of vertical resolution.

combinations will be exposed at the gray-level boundaries [28]. In Fig. 9, these erroneous pixel combinations are outlined by gray dashed lines. In Fig. 9(b), the photoresist exposes deeper because the misaligned region is more transparent than the intended design, but in Fig. 9(c), the case is reversed.

Misalignments of 0.1 and 0.2 μm were simulated on a previously designed wedge structure. First, the dose profile was calculated using the pixel sizes from the mask design and (5). Then, the resulting simulated structure was determined using the dose profile with the calibration curve. This simulation technique first simulated exposing both mask profiles with no misalignment. Then, the same process was repeated, but the second mask was shifted by 0.1 or 0.2 μm relative to the first mask. Since this misalignment is less than the 2.6-μm pixel spacing, diffraction was approximated by interpolating the pixel structure to a 0.1-μm grid. The dose was calculated at each super-resolution grid point, and then, the data spacing was restored by averaging every 26 points.

The profile roughness was observed to increase with the simulated misalignment (Fig. 10). Furthermore, larger deviations occurred when the difference in size between adjacent pixels across a gray-level interface was large. However, if the difference in pixel size was less than 0.7 μm, the roughness caused by misalignment was observed to be below the average step height for a perfectly aligned exposure. Using this result, a design rule was implemented into the mask layout algorithms. As the mask pattern is generated, the gray levels with an adjacent pixel size difference greater than 0.7 μm are removed and replaced with the closest gray level that satisfies the design rule. A wedge structure was designed and simulated using the new mask layout algorithms. The results show a dramatically reduced roughness in the presence of some misalignment, as shown in Fig. 11. While the roughness is significantly reduced, the average vertical step size is only increased from 0.02 to 0.03 μm when the design rule is applied.

C. Further Applications

The double-exposure technique could theoretically be applied to any grayscale mask technology to increase the number of possible gray levels. Continuous-tone masks would see little gain, as the vertical resolution is already sufficiently high. However, both pixelated and planar masks can benefit from double-exposure technology. As demonstrated, double-exposure photolithography will greatly increase the vertical

resolution of pixelated grayscale photolithography using high-resolution chrome masks. However, this technique also enables the use of lower resolution mask writers that can only produce a small number of pixel sizes. For example, if just seven pixel sizes are possible, double-exposure photolithography would enable designs with up to 49 gray levels. This approaches the number of gray levels possible using a single high-resolution chrome mask.

In addition, the calibration technique presented here can be applied toward multiple-step photolithography. Demonstrations of this photolithography technique in the literature only use adjacent exposures instead of overlaid exposures. Using the calibration methods applied for double-exposure lithography, it would be possible to design a multiple-step exposure that would produce 2^n gray levels, instead of $1 + n$ levels, when using n masks.

VI. Conclusion

The double-exposure technique has been successfully demonstrated to improve the vertical resolution of pixelated grayscale photolithography without requiring a change in the mask fabrication technology. The average step height was reduced by an order of magnitude, and the maximum step height was reduced by a factor of two compared to a single grayscale exposure using the same set of pixel sizes. This improvement in the vertical resolution enables fabrication of more complex devices that require more precise vertical control.

While the application of the double-exposure technique enables a high-resolution pixelated chrome mask to achieve vertical resolutions of continuous-tone masks, it also makes it possible for some lower resolution mask writers to produce grayscale masks. A tool capable of writing only seven pixel sizes for a single exposure can now realize nearly as many gray levels as was previously possible with a single exposure with a high-resolution grayscale mask.

The calibration and simulation scheme presented here allows investigation of critical fabrication tolerances, such as mask alignment. Using this example, other higher order effects can be examined to further improve the technology. Design rules from these investigations can be combined into a comprehensive design tool for intelligent double-exposure grayscale mask creation toward fabrication of complex 3-D silicon MEMS devices.

Acknowledgment

References

[1] C. Waits, B. Morgan, M. Kastantin, and R. Ghodssi, "Microfabrication of 3D silicon MEMS structures using gray-scale lithography and deep reactive ion etching," *Sens. Actuators A, Phys.*, vol. 119, no. 1, pp. 245–253, Mar. 2005.
[2] P. Yao, G. J. Schneider, and D. Prather, "Three-dimensional lithographical fabrication of microchannels," *J. Microelectromech. Syst.*, vol. 14, no. 4, pp. 799–805, Aug. 2005.
[3] P. Yao, G. J. Schneider, D. Prather, E. Wetzel, and D. O'Brein, "Fabrication of three-dimensional photonic crystals with multilayer photolithography," *Opt. Express*, vol. 13, no. 7, pp. 2370–2376, Apr. 2005.
[4] B. Morgan, C. Waits, J. Krizmanic, and R. Ghodssi, "Development of a deep silicon phase Fresnel lens using gray-scale technology and deep reactive ion etching," *J. Microelectromech. Syst.*, vol. 13, no. 1, pp. 113–120, Feb. 2004.
[5] B. Wagner, H. J. Quenzer, W. Henke, W. Hoppe, and W. Pilz, "Microfabrication of complex surface topographies using grey-tone lithography," *Sens. Actuators A, Phys.*, vol. 46, no. 1–3, pp. 89–94, Jan./Feb. 1995.
[6] J. Chung and W. Hsu, "Enhancement on forming complex three dimensional microstructures by a double-side multiple partial exposure method," *J. Vac. Sci. Technol. B, Microelectron. Process. Phenom.*, vol. 25, no. 5, pp. 1671–1678, Sep./Oct. 2007.
[7] M. Tormen, L. Businaro, M. Altissimo, F. Romanato, S. Cabrini, F. Perennes, R. Proietti, H.-B. Sun, S. Kawata, and E. D. Fabrizio, "3D patterning by means of nanoimprinting, X-ray and two-photon lithography," *Microelectron. Eng.*, vol. 73/74, no. 1, pp. 535–541, Jun. 2004.
[8] J. Kim, D. C. Joy, and S.-Y. Lee, "Controlling resist thickness and etch depth for fabrication of 3D structures in electron-beam grayscale lithography," *Microelectron. Eng.*, vol. 84, no. 12, pp. 2859–2864, Dec. 2007.
[9] L. Vivien, X. L. Roux, S. Laval, E. Cassan, and D. Marris-Morini, "Design, realization, and characterization of 3-D taper for fiber/microwaveguide coupling," *IEEE J. Sel. Topics Quantum Electron.*, vol. 12, no. 6, pp. 1354–1358, Nov./Dec. 2006.
[10] F. Hu and S.-Y. Lee, "Dose control for fabrication of grayscale structures using a single step electron-beam lithographic process," *J. Vac. Sci. Technol. B, Microelectron. Process. Phenom.*, vol. 21, no. 6, pp. 2672–2679, Nov./Dec. 2003.
[11] K. Totsu, K. Fujishiro, S. Tanaka, and M. Esashi, "Fabrication of three-dimensional microstructure using maskless gray-scale lithography," *Sens. Actuators A, Phys.*, vol. 130/131, pp. 387–392, Aug. 2006.
[12] A. Bertsch, P. Bernhard, and P. Renaud, "Microstereolithography: Concepts and applications," in *Proc. IEEE Int. Conf. Emerg. Technol. Factory Autom.*, 2001, pp. 289–298.
[13] W. H. Teh, U. Dürig, G. Salis, R. Harbers, U. Drechsler, R. F. Mahrt, C. G. Smith, and H.-J. Güntherodt, "SU-8 for real three-dimensional subdiffraction-limit two-photon microfabrication," *Appl. Phys. Lett.*, vol. 84, no. 20, pp. 4095–4097, May 2004.
[14] Y. Opplinger, P. Sixt, J. M. Stauffer, P. Regnault, and G. Voirin, "One-step 3D shaping using a gray-tone mask for optical and microelectronic applications," *Microelectron. Eng.*, vol. 23, no. 1–4, pp. 449–454, Jan. 1994.
[15] C. M. Waits, A. Modafe, and R. Ghodssi, "Investigation of gray-scale technology for large area 3D silicon MEMS structures," *J. Micromech. Microeng.*, vol. 13, no. 2, pp. 170–177, Mar. 2003.
[16] B. Morgan, C. M. Waits, and R. Ghodssi, "Compensated aspect ratio dependent etching (CARDE) using gray-scale technology," *Microelectron. Eng.*, vol. 77, no. 1, pp. 85–94, Jan. 2005.
[17] B. Morgan, X. Hua, T. Iguchi, T. Tomioka, G. Oehrlein, and R. Ghodssi, "Substrate interconnect technologies for 3-D MEMS packaging," *Microelectron. Eng.*, vol. 81, no. 1, pp. 106–116, Jul. 2005.
[18] M. Woytasik, J.-P. Grandchamp, E. Dufour-Gergam, J.-P. Gilles, S. Megherbi, E. Martincic, H. Mathias, and P. Crozat, "Two- and three-dimensional microcoil fabrication process for three-axis magnetic sensors on flexible substrates," *Sens. Actuators A, Phys.*, vol. 132, no. 1, pp. 2–7, Nov. 2006.
[19] B. Morgan, J. McGee, and R. Ghodssi, "Automated 2-axis optical fiber alignment using gray-scale technology," *J. Microelectromech. Syst.*, vol. 16, no. 1, pp. 102–110, Feb. 2007.
[20] B. Morgan and R. Ghodssi, "Vertically-shaped tunable MEMS resonators," *J. Microelectromech. Syst.*, vol. 17, no. 1, pp. 85–92, Feb. 2008.
[21] Y.-T. Lu, C.-S. Chu, and H.-Y. Lin, "Characterization of the gray-scale photolithography with high-resolution gray steps for the precise fabrication of diffractive optics," *Opt. Eng.*, vol. 43, no. 11, pp. 2666–2670, Nov. 2004.
[22] V. Kudryashov, X.-C. Yuan, W.-C. Cheong, and K. Radhakrishnan, "Grey scale structures formation in SU-8 with e-beam and UV," *Microelectron. Eng.*, vol. 67/68, pp. 306–311, Jun. 2003.
[23] A. Epstein, "Millimeter-scale, micro-electro-mechanical systems gas turbine engines," *J. Eng. Gas Turbines Power*, vol. 126, no. 2, pp. 205–226, Apr. 2004.
[24] L. Mosher, B. Morgan, C. M. Waits, and R. Ghodssi, "Advanced techniques in 3D photolithography for MEMS," presented at the 25th Army Science Conf., Orlando, FL, Nov. 27–30, 2006.

[25] F. Dill, W. Hornberger, P. Hauge, and J. Shaw, "Characterization of positive photoresist," *IEEE Trans. Electron Devices*, vol. ED-22, no. 7, pp. 445–452, Jul. 1975.

[26] H.-H. Kim, J.-Y. Yoo, S.-W. Park, Y.-K. Kwon, I. An, and H.-K. Oh, "A practical method for extracting the photoresist exposure parameters by using a dose-to-clear swing curve," *J. Korean Phys. Soc.*, vol. 42, pp. S280–S284, Feb. 2003.

[27] L. A. Mosher, B. C. Morgan, and R. Ghodssi, "Double-exposure gray-scale technology for improved vertical resolution of 3D photoresist structures," presented at the 54th Int. Symp. American Vacuum Society, Seattle, WA, Oct. 14–19, 2007.

[28] L. A. Mosher, C. M. Waits, B. Morgan, and R. Ghodssi, "A new paradigm for high resolution 3D lithography," in *Proc. IEEE MEMS*, 2008, pp. 395–398.

Brian Morgan (S'04–M'06) received the B.S. degree in physics from Georgetown University, Washington, DC, in 2002, and the M.S. and Ph.D. degrees in electrical engineering from the University of Maryland, College Park, in 2004 and 2006, respectively.

He currently works in the Sensors and Electron Devices Directorate, U.S. Army Research Laboratory, Adelphi, MD, with a focus on MEMS power components. His main research interests are in the areas of small-scale power generation and conversion, thermal management, and microfabrication techniques.

Dr. Morgan is a member of the Sigma Xi Scientific Research Society.

Lance Mosher received the B.S. degree in physics and marine science from Eckerd College, Saint Petersburg, FL, in 2005, and the M.S. degree in electrical engineering from the University of Maryland, College Park, in 2008.

He is currently an Electronics Engineer with the Global Positioning System (GPS) Block III Program at Lockheed Martin Space Systems Company, Newtown, PA. His main research interests include 3-D MEMS fabrication, power MEMS, and new microfabrication techniques.

Christopher M. Waits (S'01) received the B.S. degree in physics from Salisbury University, Salisbury, MD, in 2000, and the M.S. and Ph.D. degrees in electrical engineering from the University of Maryland, College Park, in 2003 and 2008, respectively.

Since 2004, he has been with the Sensors and Electron Devices Directorate, U.S. Army Research Laboratory, Adelphi, MD, as an Electronics Engineer. His main research interests include MEMS components and systems focused on power and energy generation and conversion (Power MEMS), MEMS tribology and bearing mechanisms, and new microfabrication techniques.

Dr. Waits was the recipient of the Physics Excellence Award from Salisbury University in 2000, the Graduate Assistance in Areas of National Need Fellowship from 2001 to 2003, and the Department of the Army Research and Development Achievement Award for Technical Excellence in 2007.

Reza Ghodssi (S'92–M'96) is the Herbert Rabin Distinguished Associate Professor and the Director of the MEMS Sensors and Actuators Laboratory, Department of Electrical and Computer Engineering, and the Institute for Systems Research, University of Maryland (UMD), College Park. He is also affiliated with the Fischell Department of Bioengineering, the Maryland NanoCenter, the University of Maryland Energy Research Center, and the Materials Science and Engineering Department, UMD. He has over 62 scholarly publications. He is the Coeditor of the *Handbook of MEMS Materials and Processes* (to be published in 2009) and is an Associate Editor for the JOURNAL OF MICROELECTROMECHANICAL SYSTEMS and *Biomedical Microdevices*. His research interests include the design and the development of microfabrication technologies and their applications to microdevices/nanodevices and systems for chemical and biological sensing, small-scale energy conversion, and harvesting.

Dr. Ghodssi was the recipient of the 2001 UMD George Corcoran Award, the 2002 National Science Foundation CAREER Award, and the 2003 UMD Outstanding Systems Engineering Faculty Award. He is the Cofounder of MEMS Alliance in the greater Washington area. He is a member of the American Vacuum Society, the Materials Research Society, the American Society for Engineering Education, and the American Association for the Advancement of Science.